Springer

KSME

Journal of Mechanical Science and Technology 26 (1) (2012) 205~212
www.springerlink.com/content/1738-494x
DOI 10.1007/s12206-011-0916-8

Adaptive feedforward control of ionic polymer metal composites with disturbance cancellation †

Seonhyeok Kang[1], Woojin Kim[1], H. Jin Kim[1,*] and Jaegyun Park[2,*]

[1]*School of Mechanical and Aerospace Engineering, Seoul National University, Seoul, 151-742, Korea*
[2]*Department of Civil and Environmental Engineering, Dankook University, Yongin, 448-701, Korea*

(Manuscript Received January 8, 2011; Revised June 12, 2011; Accepted August 30, 2011)

Abstract

Ionic polymer-metal composites (IPMCs) are promising candidates in various sensing and actuation applications due to their light weight, large bending, and low actuation voltage requirements. However, IPMCs are still in the early stage of development, and their bending response can vary widely depending on various factors such as fabrication process, water content, temperature, and contact with electrodes. To control IPMCs in a predictable manner and to minimize the effects of plant uncertainty and external disturbances, a precise and robust control scheme is required. In the present work, a three-part adaptive feedforward control architecture is employed for IPMC deflection control. First, adaptive identification is performed to identify changes in the dynamic behavior over time and in the input voltage using a gradient descent method. Second, an adaptive feedforward controller is implemented to control the dynamic response of the plant, where the IPMC displacement is observed and is used to adjust the parameters of the controller. Third, noise and disturbance cancelling is performed using an additional adaptive canceller, which does not affect the system dynamics. Our results show that the adaptive identification and feedforward controller with disturbance cancellation using the gradient descent method provides accurate tracking performance under plant variation and disturbance. Especially, the fast convergence speed of the proposed technique makes it practical for online control.

Keywords: Ionic polymer-metal composites; Disturbance cancellation; Adaptive feedforward control

1. Introduction

Ionic polymer-metal composites (IPMCs) are electroactive polymers that can generate a large bending motion with relatively low activation voltage [1, 2]. IPMCs have received much interest as candidates in various sensing and actuation applications such as micro-manipulator [3], miniaturized robotic arm [4], micro-pump [5], guide-wire for catheters [6], planetary exploration [7], micro-aircraft [8], and swimming robot [9], with an additional advantage of the capability to function in aqueous environments.

Much attention has been given to the actuator characteristics of IPMCs with respect to the applied voltage. To obtain the desired bending responses from IPMC beams, various control methods including proportional-integral-derivative (PID) control [10], integrator anti-windup [11], linear quadratic regulation [12], and a genetic algorithm [13], have been applied.

However, IPMC characteristics tend to vary with temperature [14], humidity [15], surface treatments [16], and interlayer conditions [17]. The difficulty lies in the fact that these factors contribute to non-repeatability and uncertainty [18], which are inherent in the operating principles and fabrication processes of IPMCs. Improving the robustness and reliability of IPMCs will improve its potential in a wider range of applications.

To address non-repeatability and uncertainty in the response of IPMC strips, a PID with genetic optimization [19] and robust control techniques [20] have been applied. However, the PID controllers cannot guarantee robust performance, and robust controllers with fixed gains cannot deal with time-varying or nonlinear characteristics over a specified magnitude. Furthermore, their design usually involves trade-offs between nominal and robust performances.

On the other hand, adaptive controllers can be used to adjust controller gains when the system parameters vary. Previous works concerning IPMC adaptive control were mostly based on a model reference control, where a controller is designed to match the output of a pre-specified reference model. In Ref. [13], a model reference adaptive control (MRAC) architecture is presented with pole-placement control using genetic optimization strategies for tracking. In Ref. [21], an efficient control system based on MRAC is presented to ensure repeatable

† This paper was recommended for publication in revised form by Associate Editor Junzhi Yu

* Corresponding author. Tel.: +82 31 8005 3473, Fax.: +82 2 877 2662
E-mail address: hjinkim@snu.ac.kr, jpark@dankook.ac.kr

Table 1. Properties of IPMC strips.

Width	Length	Thickness	Resistance	Capacitance
5 mm	20 mm	0.7 mm	5–20 Ω /square	400–800 μF/cm^2

responses even when the dynamic behavior of the IPMC strip changes with time. Furthermore, dead zone and parameter projection schemes are implemented to reduce the effects of perturbations in the parameter estimation process.

In the present paper, a three-part adaptive control architecture for IPMCs is employed. We first develop a dynamic model which captures time-varying characteristics by estimating the IPMC dynamics of the plant using the gradient descent method. Based on this identified model, an adaptive feedforward controller is designed for the precision position control of IPMC strips. A noise cancellation technique is also applied to mitigate the effects of plant disturbances. Using the proposed techniques, the output of the identified reference model converges to the plant output at a speed sufficient for the online adaptation structure.

In the following section, the experimental setup is described. Section 3 presents a model of the IPMC time response and an adaptive identification technique. Section 4 describes an adaptive feedforward controller designed to track the desired output as closely as possible in a mean-squared-error sense, and a noise cancellation scheme for sensor noise and disturbance. Section 5 presents the identification and control results. Finally, Section 6 summarizes the present paper with concluding remarks.

2. Experimental setup

The IPMC specimens used in the present study were fabricated using a hot-pressing method to improve the generating force. Four sheets of Nafion-117 from Dupont were stacked in this procedure. Argon plasma treatment was performed to enhance the adhesion strength between the metal electrode and the parylene. The specimens were then coated with parylene to suppress water evaporation.

The IPMC samples were cut into 20 mm × 5 mm × 0.7 mm beams for actuation tests (Table 1). According to four-point measurements, their resistance ranges from 5 to 20 Ω/square, and their capacitance is between 400 and 800 μF/cm^2. Fig. 1 shows the setup used for measuring the IPMC displacement in an acrylic container in this experiment. As shown in the zoomed-in view, the deflection of the IPMC strip was measured at a location of 5 mm inward from the bottom tip of the strip using a reflex sensor (CP25QXVT80 by Wenglor). A feedback controller is employed in computing the proper actuation voltage to control the deflection of the specimen, and a PC with an analog I/O board provides the voltage for the IPMC. The high electric conductivity of the IPMC strip requires high current to keep the desired voltage, for which the output current from an I/O board may be insufficient. To avoid this situation, power op-amp and current boost circuit are implemented on-board between the I/O board and the IPMC. The overall signal flow in the experimental setup is shown in Fig. 2.

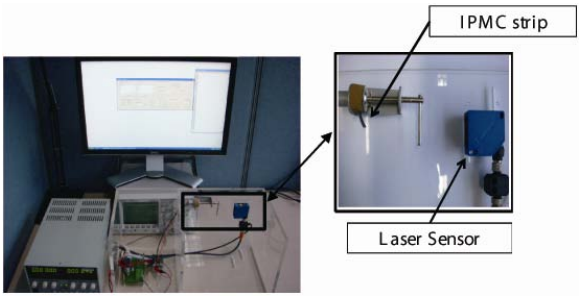

Fig. 1. The experimental setup consisting of a laser sensor, an I/O board, and a controller.

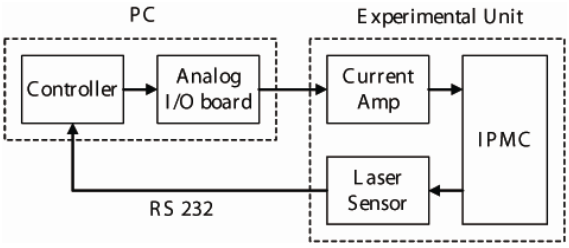

Fig. 2. Flow chart for the correction of the roll-forming process design.

3. Adaptive plant identification

The first step in the adaptive feedforward control design is to obtain an adaptive plant model that captures the dynamics of the system. The design may be derived from physics by analyzing the system and determining a set of differential equations which explains its dynamics. However, as mentioned in Section 1, an accurate plant model of IPMCs is difficult to obtain without addressing the inherent issue of low repeatability and uncertainty.

In the present study, the system is considered as a black box that can be identified in real time, implementing some sort of universal transfer function. It may be tuned by adjusting its internal parameters to capture the dynamics of the system. This is a straightforward application of adaptive filtering techniques [22].

A method for adaptive system identification is employed as shown in Fig. 3. The goal is to obtain a dynamic process $\hat{P}$ that approximates the true IPMC dynamics denoted by P. At each time step, the input signal u_k (voltage in our case) is given to the system P, and the output y_k (IPMC displacement) is measured. The adaptive plant model $\hat{P}$ is also excited with u_k, and its output $\hat{y}_k$ is computed. The plant modeling error $e_k = y_k - \hat{y}_k$ is used by the adaptation algorithm.

In our setting, the output $\hat{y}_k$ of the adaptive plant model at time k is a function of the following form:

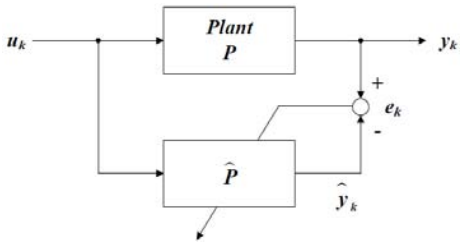

Fig. 3. Adaptive plant identification.

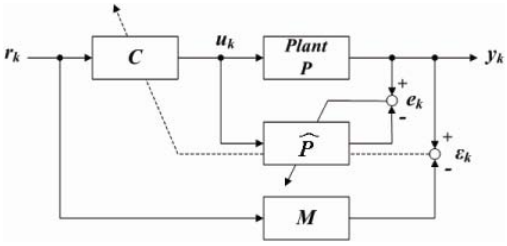

Fig. 4. Feedforward control structure.

$$\hat{y}_k = W_k U_k \tag{1}$$

where W_k is a vector containing weight parameters, and U_k is a column vector consisting of the previous input and output histories.

$$W_k \triangleq [w_1 \; w_2 \; \cdots \; w_{n+m+1}] \tag{2}$$

$$U_k \triangleq [u_k \; u_{k-1} \; \cdots \; u_{k-n} \; \hat{y}_{k-1} \; \hat{y}_{k-2} \; \cdots \; \hat{y}_{k-m}]^T \tag{3}$$

Here $w_1, w_2, \cdots, w_{n+m+1}$ are the weight parameters that need to be updated to minimize the following cost function:

$$J_k \approx \frac{1}{2} e_k^T e_k. \tag{4}$$

The values of *n* and *m* in Eqs. (2) and (3) are decided by trial and error with insights from a continuous-time black-box model [19]. To adapt the weight vector W_k, a simple gradient descent optimization is used, that is, the change in the weights ΔW_k is calculated as

$$\Delta W_k^T = -\eta \frac{dJ_k}{dW_k}. \tag{5}$$

The positive constant η is the learning rate parameter which controls the step size in the direction of the negative gradient. Using the standard vector calculus, dJ_k / dW_k can be calculated as

$$\frac{dJ_k}{dW_k} = -e_k^T \frac{d\hat{y}_k}{dW_k}. \tag{6}$$

To compute the weight update formula in Eq. (5), it is necessary to find $d\hat{y}_k / dW_k$. Using Eqs. (1) and (3), $d\hat{y}_k / dW_k$ can be rewritten as

$$\frac{d\hat{y}_k}{dW_k} = \frac{\partial \hat{y}_k}{\partial W_k} + \sum_{i=0}^{n} \frac{\partial \hat{y}_k}{\partial u_{k-i}} \frac{du_{k-i}}{dW_k} + \sum_{i=1}^{m} \frac{\partial \hat{y}_k}{\partial \hat{y}_{k-i}} \frac{d\hat{y}_{k-i}}{dW_k}. \tag{7}$$

The first term $\partial \hat{y}_k / \partial W_k$ in Eq. (7) is the direct effect of a change in the weights on $\hat{y}_k$. In most cases, it is computed by vectorizing (1) to get $\hat{y}_k = \left[U_k^T \otimes I\right] W_k$, where $\otimes$ is the Kronecker matrix product. However, $\hat{y}_k$ is scalar in our setting; thus, $\partial \hat{y}_k / \partial W_k$ can be simply expressed as

$$\frac{\partial \hat{y}_k}{\partial W_k} = U_k^T. \tag{8}$$

In the second term of Eq. (7), du_{k-i} / dW_k is zero because $u_k, \cdots, u_{k-n}$ is independent of W_k. The final term is broken down into two parts. The first part, $\partial \hat{y}_k / \partial \hat{y}_{k-i}$, is an element of W_k which multiplies $\hat{y}_{k-i}$, that is, w_{n+i+1}. The second part, $d\hat{y}_{k-i} / dW_k$, is simply a previously computed and stored value of $d\hat{y}_k / dW_k$. When the adaptation loop is started, the initial values for $d\hat{y}_k / dW_k$ are set to zero for $k = 0, -1, -2, \cdots$.

4. Adaptive controller design

This section describes the design of the adaptive controller. In Section 4.1, we describe the structure of the adaptive controller and the parameter update rules. Section 4.2 presents the noise cancellation scheme.

4.1 Adaptive controller design

Fig. 4 shows the overall control architecture, which consists of the adaptive identified model $\hat{P}$, the adaptive feedforward controller *C*, and a reference model *M*. The aim of the adaptive control is to make the controlled system *PC* approximate the user-defined reference model *M* as closely as possible in the least mean square error sense. For this, both the plant model $\hat{P}$ and the controller *C* can be adapted. In that sense, the series combination of *C* and $\hat{P}$ can be seen as a single adaptive filter. In our setting, *M* is simply chosen as 1 so that the error term represents the deviation from the reference displacement, that is, $\varepsilon_k = y_k - r_k$. In general, *M* can be designed to represent a fixed-order linear system with a desired response that meets design specifications.

To adapt the feedforward controller *C* and minimize the squared system error over a certain trajectory, and to simultaneously minimize the control effort, the cost function is set as

$$J_{C_k} = \frac{1}{2} \varepsilon_k^T \varepsilon_k + h(u_k, u_{k-1}, \cdots, u_{k-r}) \tag{9}$$

where the differentiable function $h(\cdot)$ is used to penalize the excessive control effort.

Assuming that we have the adapted plant model $\hat{P}$ with

the weight vector W from Section 3, we can state that

$$u_k = W_{C_k} R_k$$
$$y_k \approx \hat{y}_k = W_k U_k$$

where W_{C_k} is the controller weight vector, and

$$R_k \triangleq \left[r_k, r_{k-1}, \cdots r_{k-m}, u_k, u_{k-2}, \cdots, u_{k-p}\right]^T$$
$$U_k \triangleq \left[u_k, u_{k-1}, \cdots u_{k-n}, \hat{y}_{k-1}, \hat{y}_{k-2}, \cdots, \hat{y}_{k-q}\right]^T$$

with the weighting vector W_k of the compatible dimension. As is typical for the gradient descent derived in Section 3, the controller weights W_{C_k} can be updated in the direction of the negative gradient of the cost functional

$$\Delta W_{C_k}^T = -\eta \frac{dJ_{C_k}}{dW_{C_k}}$$
$$= \eta \left[\varepsilon_k^T \frac{d\hat{y}_k}{dW_{C_k}} - \sum_{j=0}^{r} \left(\frac{\partial h(u_k, u_{k-1}, \cdots, u_{k-r})}{\partial u_{k-j}} \right)^T \left(\frac{du_{k-j}}{dW_{C_k}} \right) \right]. \quad (10)$$

Using the chain rule, du_k / dW_{C_k} and $d\hat{y}_k / dW_{C_k}$ in Eq. (10) can be calculated as

$$\frac{du_k}{dW_{C_k}} = \frac{\partial u_k}{\partial W_{C_k}} + \sum_{j=1}^{p} \frac{\partial u_k}{\partial u_{k-j}} \frac{du_{k-j}}{dW_{C_k}} \quad (11)$$

$$\frac{d\hat{y}_k}{dW_{C_k}} = \sum_{j=0}^{n} \frac{\partial \hat{y}_k}{\partial u_{k-j}} \frac{du_{k-j}}{dW_{C_k}} + \sum_{j=1}^{q} \frac{\partial \hat{y}_k}{\partial \hat{y}_{k-j}} \frac{d\hat{y}_{k-j}}{dW_{C_k}}. \quad (12)$$

Eq. (11) is similar in form to Eq. (7) and is computed in the same way. The first terms of each summation in Eq. (12), $\partial \hat{y}_k / \partial k_{k-j}$ and $\partial \hat{y}_k / \partial \hat{y}_{k-j}$, comprise the columns of W_k corresponding to u_{k-j} and $\hat{y}_{k-j}$, that is, w_{j+1} and w_{n+j+1}, respectively. The next terms of each summation, and $d\hat{y}_{k-j} / dW_{C_k}$, are the current or previously computed and saved values of du_k / dW_{C_k} and $d\hat{y}_k / dW_{C_k}$. Note also that $\partial h(\cdot) / \partial u_{k-j}$ depends on the user-defined function $h(\cdot)$.

4.2 Adaptive noise cancellation

Thus far, we have described how to adaptively model the plant dynamics and how to use the plant model to adapt a feedforward controller. Using this controller, the plant output tracks the desired output as closely as possible in a mean-squared-error sense. It remains to be seen what can be done to mitigate the plant disturbance. In the present study, the weight update algorithm, which is quite similar with that described in Section 4.1, is used.

Fig. 5 depicts the structure of the noise cancellation method. Let u_k be the output of the controller, and let $\tilde{u}_k$ be the output of the noise canceller *X*. Likewise, let $\hat{y}_k$ be the estimated value from the plant model copy $\hat{P}_{COPY}$, and let W_{X_k} be the

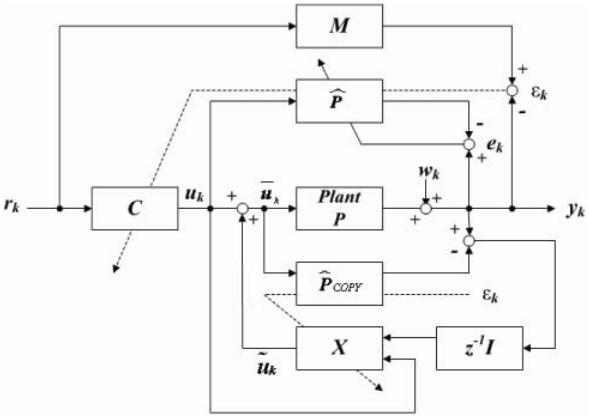

Fig. 5. Overall controller structure including the noise cancellation block *X*.

weights of the noise canceller *X* at time *k*. Then,

$$\tilde{u}_k = W_{X_k} \tilde{U}_k$$
$$y_k \approx \hat{y}_k = W_k \bar{U}_k$$

where

$$\tilde{U}_k \triangleq \left[\tilde{u}_{k-1}, \cdots, \tilde{u}_{k-m}, \hat{w}_{k-1}, \cdots, \hat{w}_{k-q}, u_k, \cdots u_{k-r}\right]^T$$
$$\bar{U}_k \triangleq \left[\hat{y}_{k-1}, \cdots, \hat{y}_{k-n}, \bar{u}_k, \cdots \bar{u}_{k-p}\right]^T$$

and $\bar{u}_k = u_k + \tilde{u}_k$ denotes the input to the plant. The weight update for the noise canceller, $\Delta W_{X_k}^T = -\eta \varepsilon_k^T d\hat{y}_k / dW_{X_k}$, can be performed using the following equations:

$$\frac{d\bar{u}_k}{dW_{X_k}} = \frac{du_k}{dW_{X_k}} + \frac{d\tilde{u}_k}{dW_{X_k}}$$
$$= \frac{\partial \tilde{u}_k}{\partial W_{X_k}} + \sum_{j=1}^{m} \frac{\partial \tilde{u}_k}{\partial \tilde{u}_{k-j}} \frac{d\bar{u}_{k-j}}{dW_{X_k}} \quad (13)$$

$$\frac{d\hat{y}_k}{dW_{X_k}} = \sum_{j=0}^{p} \frac{\partial \hat{y}_k}{\partial \bar{u}_{k-j}} \frac{d\bar{u}_{k-j}}{dW_{X_k}} + \sum_{j=1}^{n} \frac{\partial \hat{y}_k}{\partial \hat{y}_{k-j}} \frac{d\hat{y}_{k-j}}{dW_{X_k}}. \quad (14)$$

In practice, depending on the plant to be controlled, it might be difficult to adapt the controller *C* and the noise canceller *X* simultaneously. It is better to adapt the plant model to near convergence, $y_k \approx \hat{y}_k$, before connecting the noise canceller output to the plant input. If the performance of the noise canceller is not satisfactory, fine-tuning the learning rate η, the step size, and the number of parameters such as m, n, p in Eqs. (13) and (14) is also needed.

5. Results

This section demonstrates the performance of the adaptive feedforward control algorithm. In Section 5.1, the experimental data for the off-line plant identification are presented. The resulting mathematical models are also described. In Section

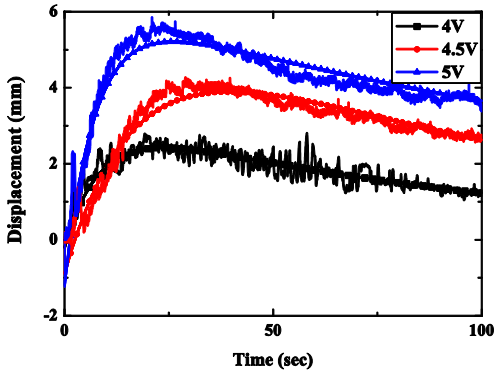

Fig. 6. IPMC beam displacements under actuation voltages of 4, 4.5, and 5 V DC, and fitted curves versus time represented by (15).

5.2, the effectiveness of the adaptive identifications is evaluated. Section 5.3 describes the performance of the three-part adaptive feedforward controller in both the presence and the absence of noise.

5.1 Plant description

To obtain the plant model P, the open-loop time histories of IPMC deflection were measured with respect to the applied voltage using the experimental setup described in Section 2. Fig. 6 presents the time responses of the same IPMC sample with different applied voltages of 4, 4.5, and 5 V DC, measured about 20 min apart.

As shown in Fig. 6, the steady-state tip displacement of IPMCs and the applied voltages do not obey the linear relationship, unlike the actuation model in [14]. This means that the parameters in Eq. (15) also depend on the applied voltage, and the standard linear invariant model cannot accurately describe the IPMC bending behavior.

As each open-loop time-response to the step input voltage shows exponential combinations, the IPMC data can be approximated in the following form. In Ref. [23], the similar form of Eq. (15) is suggested. The parameters y_1, y_2, y_3, a, b, and c are estimated using least squares.

$$y(t)=y_1e^{-at}+y_2e^{-bt}+y_3e^{-ct} \tag{15}$$

Taking the Laplace transformation of the output and input equations, we get

$$Y(s)=\frac{y_1}{s+a}+\frac{y_2}{s+b}+\frac{y_3}{s+c} \tag{16}$$

$$U(s)=\frac{applied\ step\ voltage}{s}. \tag{17}$$

After substituting the values of y_1, y_2, y_3, a, b, and c obtained previously, the transfer function from the input voltage to the displacement of the IPMC strip can be determined by taking the ratio of $Y(s)$ and $U(s)$. We used it as the plant model P at a particular voltage.

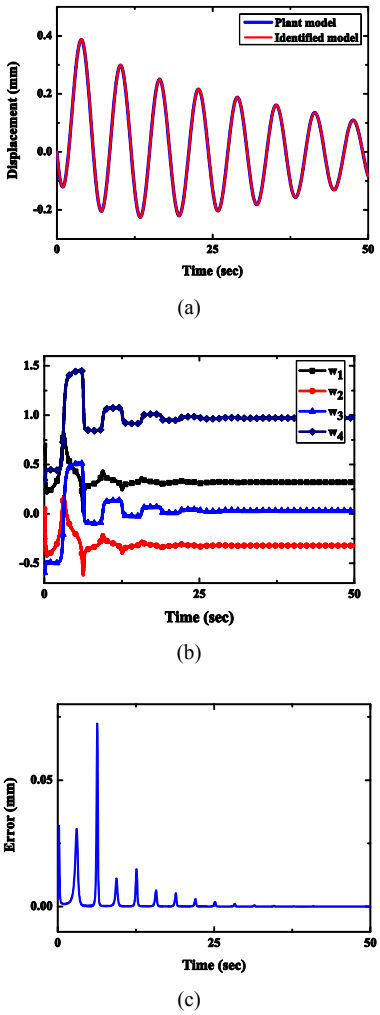

Fig. 7. (a) Adaptive identification without measurement noise; (b) Updates of the weights W; (c) Root-mean-square error between the outputs of the plant model P and the identified model $\hat{P}$.

5.2 Adaptive identification

Plant identification was performed in the absence of measurement noise, starting with random initial weight W in Eq. (2). To consider the uncertainty and variation of the plant model, the time-varying model in Eq. (15) was used, which represents the voltage-dependent IPMC dynamics between 4 and 5 V. A sinusoidal signal was imposed on this time-varying plant model. The simulation results are presented in Fig. 7(a). The time-update of the weights in Eq. (2) and root-mean-square error are also shown in Fig. 7(b) and Fig. 7(c), respectively. The numbers of parameters n and m in Eq. (3) were set to 1 and 2, respectively. Although it seems that many parameters could be helpful in studying the plant model, over-parametrization can deteriorate the results. The learning rate η or step size in a discrete case is a more important factor in improving the performance of the algorithm. The results show that a quite precise adaptation result was achieved even in the presence of time-varying characteristics.

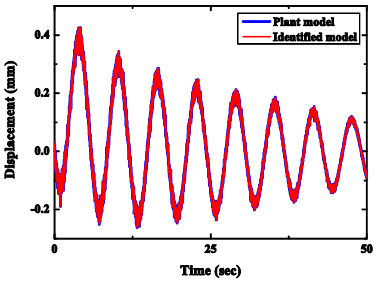

Fig. 8. Adaptive identification with measurement noise.

The results also support that the adaptive identification using the gradient descent method has a sufficiently fast convergence rate.

Fig. 8 is similar to Fig. 7; however, a plant model with a normally distributed measurement noise is adapted. As shown in Fig. 8, the measurement noise added to the plant model P is accumulated to affect the output of the adapted plant $\hat{P}$. The fact that plant adaptation rules do not use information about noise leads to biased solutions. To acquire accurately adapted data, we need to cancel the noise as described in Section 4.2. This will be further addressed in Section 5.3.

5.3 Feedforward controller

After identifying the plant model P in the absence of measurement noise, the controller was trained to perform feedforward control. The identified plant is imposed by a sinusoidal command to demonstrate the performance of the controller. Fig. 9(a) shows the tracking results, where the IPMC displacement is almost identical to the command. The control input used is shown in Fig. 9(b). Results indicate that the reference-tracking performance is satisfactory and the control inputs remain within the design specifications.

To test the noise-cancelling algorithm, measurement noise was added to the plant outputs and a sequence of step commands was imposeds. Fig. 10(a) compares the time responses with and without noise cancellation. Fig. 10(b) shows the control input used. When the noise canceller is employed, slight performance degradation is noticeable in that the settling time is increased. However, we can confirm that the disturbance canceller removes the measurement noise effectively, resulting in near-perfect tracking even in the presence of noise.

6. Conclusion

In the present study, an adaptive feedforward controller was employed for the precision control of IPMCs. Unlike conventional feedback controllers, the proposed adaptive feedforward controller can separately perform three types of control tasks: identification of the IPMC model, control of the IPMC beam, and noise cancellation. The adaptive plant identification can capture the time- or input-dependent dynamics of the plant accurately. The gradient descent method employed to adapt the weights of the feedforward controller showed satisfactory

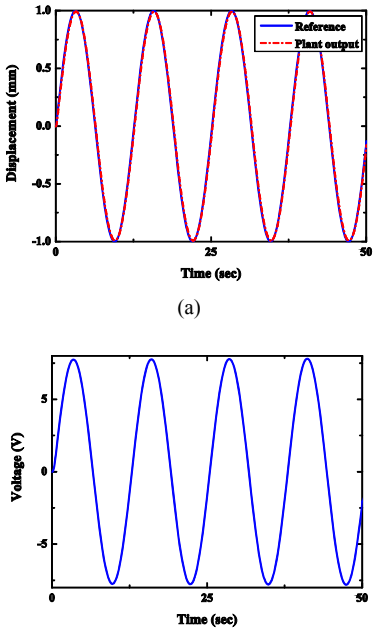

Fig. 9. (a) Reference-tracking performance for a sinusoidal trajectory without noise consideration; (b) Control input used.

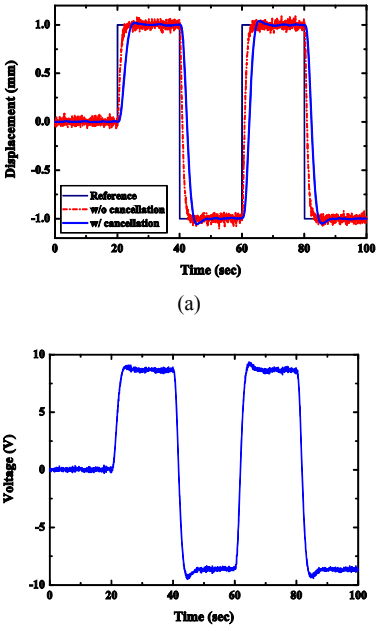

Fig. 10. (a) Tracking Performance for a square trajectory with noise cancellation (solid) and without noise cancellation (dash-dot); (b) Control input used.

reference-tracking performance and fast convergence sufficient for real-time implementation. A noise cancellation algorithm was also added to the employed controller, providing tolerance against sensor noise or external disturbance. This three-part adaptive feedforward controller will be useful for a

wider range of actuator applications that require precise control of actuators with inherent time-varying or parameter-dependent properties.

Acknowledgment

This work was partially supported by the Institute of Advanced Aerospace Technology at Seoul National University, Korea, under the Korea Research Foundation Grant funded by the Korean Government (2010-0027651). The authors would like to thank Jinho Kim for his assistance in editing.

References

[1] M. Shahinpoor, Conceptual design, kinematics and dynamics of swimming robotic structures using ionic polymeric gel muscles, *Smart Mater. Struct*., 14 (1992) 91-94.

[2] K. Oguru, Y. Kawami and H. Takenaka, Bending of an ion-conducting polymer film-electrode composite by an electric stimulus at low voltage, *Trans. J. of Micicromachine Society,* 5 (1992) 27-30.

[3] M. Shahinpoor and K. Kim, Ionic polymer-metal composite: IV. Industrial and medical applications, *Smart Mater. Struct*., 14 (2005) 197-214.

[4] K. Kim and S. Tadokoro, *Electroactive Polymers for Robotic Applications,* Springer London (2007).

[5] S. Lee and K. Kim, Design of IPMC actuator-driven valveless micropump and its flow rate estimation at low Reynolds numbers, *Smart Mater. Struct*., 15 (2006) 1103-1109.

[6] M. Ju, P. Fung, C. Lin, Y. Hong, C. Chung and T. Wu, Cardiac Catheter With Variable Head Curvature Actuated By IPMC (Ionic Polymer-Metal Composite), *Proceedings of 20th Congress of the International Society of Biomechanics, Cleveland*, OH, USA (2005).

[7] Y. Bar-Cohen, Electroactive polymers (EAP) as actuators for potential future planetary mechanisms, *NASA/DoD Conference on Evolvable Hardware* (2004).

[8] A. Colozza, M. Shahinpoor, P. Jenkins, C. Smith, K. Isaac and T. DalBello, Solid state aircraft concept overview, *Proceedings of NASA/DoD Conference on Evolvable Hardware* (2004).

[9] N. Kamamichi, M. Yamakita, K. Asaka and Z. Luo, A snake-like swimming robot using IPMC actuator/sensor, *IEEE International Conference on Robotics and Automation* (2006).

[10] R. Richardson, M. Levesley, M. Brown, J. Hawkes, K. Watterson and P. Walker, Control of ionic polymer metal composite, *IEEE/ASME Trans. Mechatronics,* 8 (2003) 245-253.

[11] K. Yun and W. Kim, Microscale position control of an electroactive polymer using an anti-windup scheme, *Smart Mater. Struct*., 15 (2006) 924-930.

[12] K. Mallavarapu, Feedback control of ionic polymer actuators, *Master's thesis,* Virginia Polytechnic Institute and State University (2001).

[13] B. Lavu, M. Schoen and A. Mahajan, Adaptive intelligent control of ionic polymer-metal composites *Smart Mater.* Struct., 14 (2005) 466-474.

[14] G. Bufalo, L. Placidi and M. Porfiri, A mixture theory framework for modeling the mechanical actuation of ionic polymer metal composites, *Smart Mater. Struct*., 17 (2008) 045010.

[15] M. Shahinpoor and K. Kim, Ionic polymer-metal composited: I. fundamentals, *Smart Mater. Struct.,* 10 (2001) 819-833.

[16] S. Kim, I. Lee and Y. Kim, Performance enhancement of IPMC actuator by plasma surface treatment, *Smart Mater. Struct*., 16 (2007) N6-N11.

[17] J. Paquette, K. Kim, D. Kim and W. Yim, The behavior of ionic polymer-metal composites in a multi-layer configuration, *Smart Mater. Struct*., 14 (2005) 881-888.

[18] C. Kothera, Micro-Manipulation and Bandwidth characterization of Ionic Polymer Actuators, *Master's thesis,* Virginia Polytechnic Institute and State University (2002).

[19] H. Jin Kim, J. Shin, S. Kang, S. J. Kim and M. Tahk, Ionic electroactive polymer control using co-evolutionary optimization, *IET Electronics Letters,* 43 (2007) 859-860.

[20] S. Kang, J. Shin, S. J. Kim, H. Jin Kim and Y. H. Kim, Robust control of ionic polymer-metal composites, *Smart Mater. Struct*., 16 (2007) 2457-2463.

[21] J. Brufau-Penella1, K. Tsiakmakis, T. Laopoulos and M. Puig-Vidal, Model reference adaptive control for an ionic polymer metal composite in underwater applications, *Smart Mater. Struct*., 17 (2008) 045020.

[22] G. L. Plett, Adaptivce inverse control of unmodeled stable SISO and MIMO linear systems, *International Journal of Adaptive Control and Signal Processing*, 16 (2002) 243-272.

[23] N. Bhat and W. J. Kim, Precision force and position control of an ionic polymer metal composite, *Proc. of the IMechE Part I: J. Systems and Control Engineering,* 16 (2004) 421-432.

Seonhyeok Kang received B.S. and M.S. degrees in aerospace engineering from the University of Ulsan and the Seoul National University, Korea, in 2006 and 2008, respectively. He is currently pursuing the Ph.D degree in mechanical and aerospace engineering from the Seoul National University, Seoul, Korea. His research interests include robust control of smart materials, pursuit-evasion games, and missile guidance and control.

Woojin Kim received his B.S. degree in electrical engineering from Korea Advanced Institute of Technology, Korea, in 2008. He is currently pursuing a Ph.D in mechanical and aerospace engineering from the Seoul National University, Seoul, Korea. His research interests are controls of smart materials, coordination and applications of networked systems.

H. Jin Kim received her B.S. degree in mechanical engineering from Korean Advanced Institute of Technology, Korea, in 1995, and M.S. and Ph.D degrees from the University of California, Berkeley, USA, in 1999 and 2001, respectively. From 2002 to 2004, she was a postdoctoral researcher and lecturer in the department of Electrical Engineering and Computer Sciences at University of California, Berkeley. In 2004, she joined the School of Mechanical and Aerospace Engineering at Seoul National University as an Assistant Professor, where she is currently an Associate Professor. Her research interests are robotics and intelligent control.

Jaegyun Park received B.S. and M.S degrees in civil engineering from Seoul National University, Korea, in 1993 and 1995, respectively. He received his Ph.D from the University of California, Berkeley, USA, in 2002. From 2002 to 2003, he was a postdoctoral researcher in the Structural Mechanics division at the University of California, Berkeley. In 2004, he joined Department of Civil & Environmental Engineering at Dankook University, Korea, as a Professor. His major research area is material modeling and nonlinear structural analysis.